

Advances in Astronomical UV Image Sensors and Associated Technologies

Charles L. Joseph

Dept. of Physics and Astronomy
Rutgers, The State University of New Jersey
Piscataway, NJ 08855-0849
cjoseph@physics.rutgers.edu

Abstract

Large-format ultraviolet image sensors have been and are actively being developed for a variety of space-borne astronomy missions. The detector is historically one of the most problematic parts of any astronomical spacecraft and it plays a critical role in the overall capability of the instrument. There are numerous detector systems with none being ideal for all applications. This paper focuses on the physical processes responsible for the inherent strengths and weaknesses of a few important UV image sensors as well as the recent technological progress that has been made to improve performance of these devices.

Key Words: UV Detectors, MCP, EBCCD, GaN, GaAlN

An Invited Paper for SPIE Conference 2000 — Photodetectors: Materials and Devices II.
This research was supported in part by grant NAGW-5045 from the National Aeronautics
and Space Administration to Rutgers University

I. INTRODUCTION

Although this paper provides comparative analysis between various ultraviolet (UV) detector technologies, it is not a comprehensive review but instead focuses only on a relatively few important detector systems. General reviews of the subject^{1,2} have been given elsewhere as well as for the extreme ultraviolet³. Similarly, photon counting detectors⁴ which dominate UV/Far-UV/Extreme-UV sensor technology and the important subset based on the microchannel plate (MCP)⁵ have been reviewed elsewhere. NASA's short- and long-term requirements for new UV sensors and the corresponding new technologies for the 21st century can be found in a technology development study led by the Jet Propulsion Laboratory called Astrotech 21^{6,7}. The scope of the present paper shall be to build primarily upon the review of Joseph², emphasizing the progress and developments that have occurred over the past two years for four detector systems that are important for UV astronomy. Hereinafter, we will restrict our attention to the wavelength interval $91.2 < \lambda < 300$ nm which includes the Far-UV, UV and near-UV, and shall discuss relevant physical processes responsible for the inherent strengths and weaknesses of these image sensors.

Each detector system has a set of unique strengths and weaknesses with none being suitable for all applications. For a telescope of a given aperture, it is usually the detector that determines the feasibility of the various scientific investigations. Thus, it is important for each new astronomical mission to choose the UV detector with the best set of inherent strengths for its particular programs. For a general-purpose UV image sensor, however, there are 5 performance requirements that are most important: 1) it should NOT be sensitive to light at optical wavelengths (commonly referred to as being solar blind), 2) it should have high Detective Quantum Efficiency (DQE), 3) it should have a high Local Dynamic Range (LDR), 4) it should have low backgrounds since noise arising from the background often dominates in faint UV observations and 5) it should have a large multiplexing capability (i.e. a large number of pixels) to maintain sufficient field of view or to record significant amounts of spectra simultaneously. Obviously, there are several other important parameters, but these are normally achieved with most detector systems and therefore are of less concern.

To summarize detector Detective Quantum Efficiencies (DQEs), Figure 1 shows the current status of common detectors. The term DQE is distinguished from ordinary QE in that it incorporates all losses including, for example, those due to the transmission efficiency of a window or the conversion efficiency of the electronics neither of which is ever perfect. A Charge Coupled Device (CCD) for instance may have a QE of 20 percent in the UV, but when it is placed behind an Alkali metal filter (Woods filter) to make it solar blind, its ultraviolet DQE typically is only 1-4%. In fact, the DQE curve in Figure 1 for the CCD plus Woods filter is for a pristine CCD/Woods combination before contamination becomes a factor.

All of the solid-line DQE curves for the MCP detectors are actual demonstrated values^{8,9,10} as is the FUV curve for the EBCCD¹¹. Plotted as dotted lines in Figure 1 are the expected UV DQEs for future EBCCDs with two types of photocathode. These EBCCD curves incorporate all known losses such as that due to the entrance window. Also plotted as a

dotted line is the expected DQE curve for a solid-state detector of GaAlN. DQE's of nearly 90% have been reported near 2500Å but little is known about the response at shorter wavelengths nor for low-light levels^{12,13}. The visible light rejection (solar blindness) measurements for GaN or GaAlN devices are not precisely determined as well.

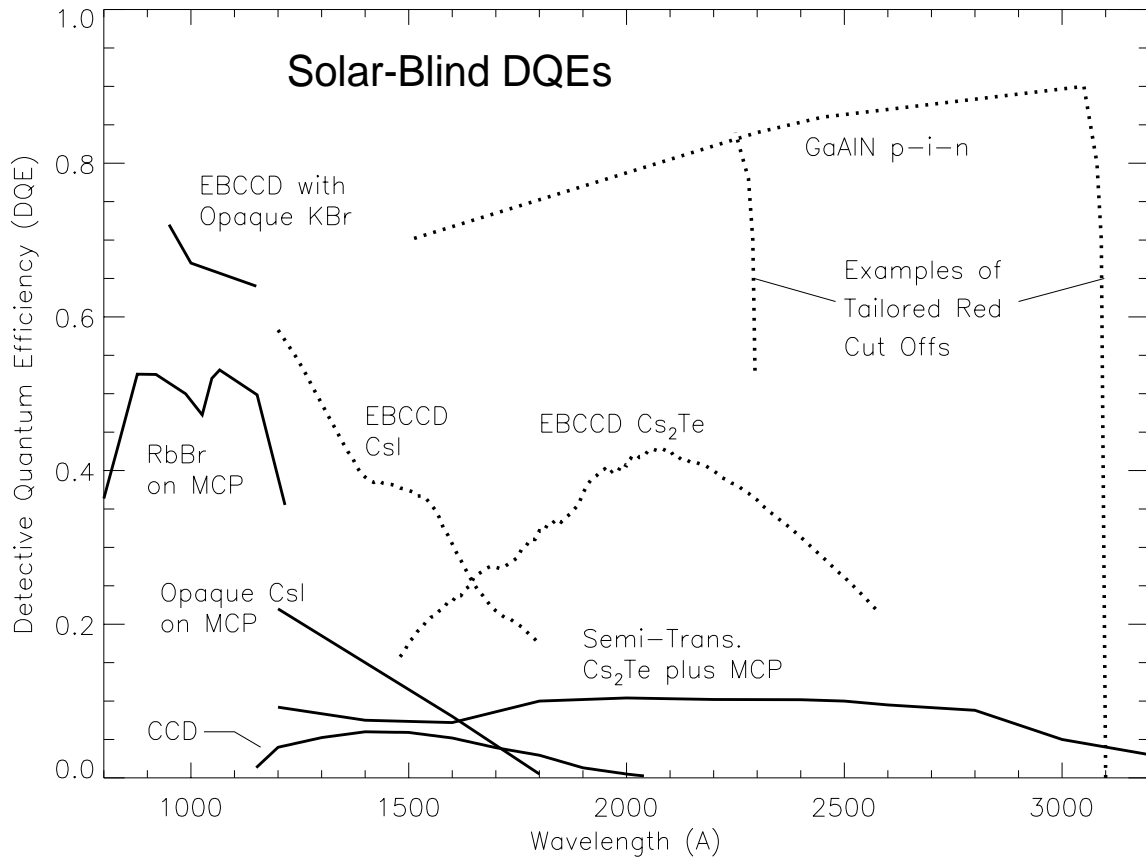


Fig. 1 showing the solar-blind UV DQEs of various detectors. Note: CCD curve is for a pristine CCD plus Woods Filter combination before contaminants become a factor.

As can be seen in Figure 1, MCP-based detectors have a significant DQE advantage over a CCD-woods filter combination, making MCP detectors one of the most successful types of ultraviolet detector. Detector systems using MCPs have been and will be used in numerous instruments spanning wavelengths ranging from X Ray through near-UV. (See references contained in a review by Joseph².) For this reason, we will adopt the MCP-based detector as our primary benchmark in the comparison to alternative detector systems.

An MCP essentially is a small, thin disk of lead-oxide glass with numerous microscopic channels, running parallel to each other from one face of the disk to the other. A schematic cross section of an MCP is pictured in Figure 2. When an electric potential is applied be-

tween the two faces, the MCP becomes an image intensifier. The device can be considered to be a compact assemblage of photomultipliers since electrons striking the walls of a pore liberate additional electrons in a continuous dynode fashion to produce an avalanche. If the potential is sufficiently large, a photoelectron then gives rise to a saturated electron cloud with a total charge falling within a narrow range that can be easily "counted" electronically. Unfortunately, MCPs have a significant surface-to-volume ratio which readily traps residual gas. Cleanliness and plate conditioning are thus important issues since MCPs are normally operated at potentials in excess of 1KeV which can cause destructive discharges.

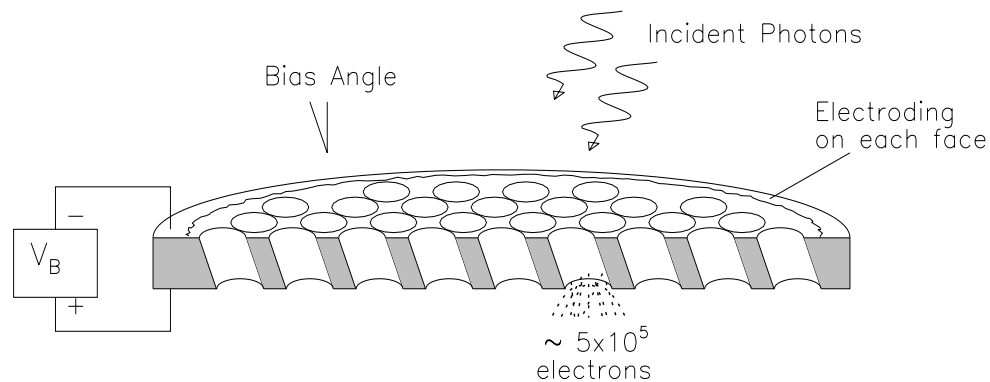


Fig. 2 a schematic drawing of a Microchannel Plate (MCP) showing half of the plate. The ratio of pore length to pore diameter (L/D) range typically from 40:1 to 120:1.

Figure 3 shows both Global- and Local- Dynamic Range envelopes for several important photoemissive devices. The distribution of light in the focal plane can significantly impact sensor performance. All envelopes in Figure 3 represent the 10% loss point^{5,8,9,14}. As an example, the distribution of light in the focal plane is shown for the medium resolution mode of STIS, denoted as "STIS: $R = 2 \times 10^4$ ". In this medium-spectral resolution mode, the distribution of light on the detector from any hot star will fall somewhere along this dashed line. The particular form of parameterization in Figure 3 stems from the fact that separate physical processes set these limits for MCP-based detectors. The GDR for most MCP-based detectors is limited by the speed of the electronics which must process each photoevent sequentially. Coincidence losses occur when the photons arrive too rapidly. The LDR, on the other hand, is set by the recharge time scale of the MCP. When light is concentrated into a small region of the detector, rapid pulsing of the MCP can lead to incomplete recharging between pulses and a corresponding sag in gain^{15,16}. Whenever the LDR is exceeded, the MCP becomes nonphotometric and introduces image distortions, especially for Z stack detectors^{15,16}.

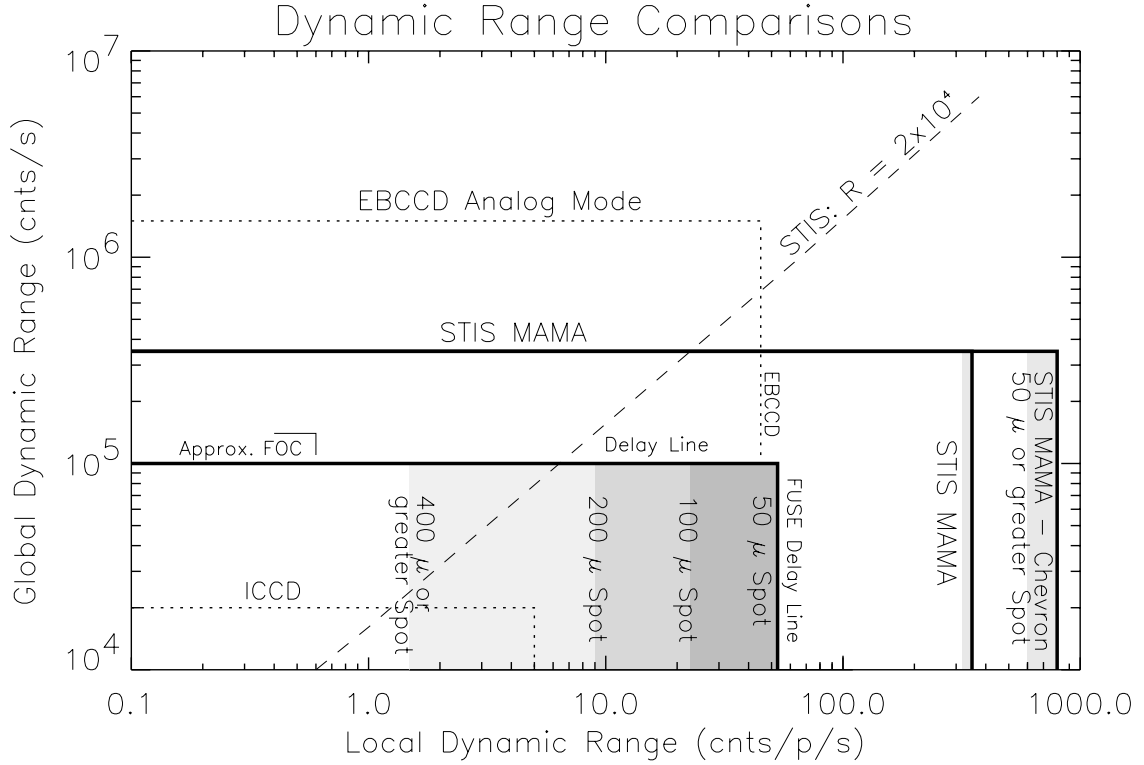


Fig. 3 showing dynamic range envelopes. All detectors have been normalized to a common size and electrical parameters (see text for details). The EBCCD Analog Mode allows multiple event pile up within a single frame time. (See Table 1 for references.)

To facilitate the comparison in Figure 3, all detector systems have been normalized to have a 1024×1024 format of square pixels each $25 \mu\text{m}$ on a side. The approximate envelope of the Faint Object Camera is shown in Figure 6 and is labeled "Approx. FOC". The electrical performances of all MCPs have been normalized to a resistance of $20 M\Omega$ for a 40 mm plate. Different detector systems based on MCPs use various numbers of MCPs, sometimes with gaps between each. As a result, the LDRs for some of these devices are strongly dependent upon the scene being recorded. The shaded regions show the limits where simultaneous loss in resolution and photometry occur as a function of spot size. The LDR for the STIS MAMA in the Chevron Configuration, for example, is independent of spot size for spot diameters of $50 \mu\text{m}$ or larger. The Delay Line, however, has an LDR over 50 for a $50 \mu\text{m}$ spot but only an LDR of < 2 cnts/pixel/second for a $400 \mu\text{m}$ or greater diameter spot. The physics behind this phenomenon will be discussed in greater detail in the next section. Table 1 gives performance comparisons for a number of parameters.

Table 1
Performance Comparisons for a Few Photoemissive Detectors

Parameter	MAMA	Delay Line	ICCD	EBCCD	Notes:
DQE	15-20%	15-20%	15-20%	50-60%	CsI at 121.6 nm
Vis. Reject.	$< 10^{-7}$	$< 10^{-6}$	$< 10^{-6}$	$< 10^{-6}$	CsI at 400 nm.
Max LDR	800 c/p/s	2-53 c/p/s	5 c/p/s	45 c/p/s	Delay Line scene dep.
Max GDR	3.5×10^5 c/s 9.0×10^5 c/s	1.0×10^5 c/s	2.0×10^4 c/s	1.5×10^6 c/s	at 10% Coinc. Loss
Array Size	1Kx1K 2Kx2K	13Kx3K	2Kx2K	1Kx1K	
Pixel Size	$25 \times 25 \mu^2$ $14 \times 14 \mu^2$	$20 \times 32 \mu^2$ $18 \times 18 \mu^2$	$7.5 \times 7.5 \mu^2$	$21 \times 21 \mu^2$	ICCD set by 1/2 of CCD pixel

References:

STIS MAMA: Joseph *et al.*^{8,9}
 FUSE Delay Line: Siegmund *et al.*¹⁴
 ICCD: Dopita¹⁷
 EBCCD: Jenkins *et al.*¹¹

2. MCP DETECTORS USING AN ANODE STRUCTURE

Microchannel plate detectors using an anode structure can be divided into subtypes based on corresponding methods to encode the electron clouds emerging from the back of the MCP. (See an invited review article by Joseph² and references therein for additional information.) Some of these encoding schemes require stacks of MCPs with the spreading of charge to multiple channels in the second or third MCP to obtain sufficient gain. One of the simplest schemes to visualize is a single resistive anode where the location of the event is encoded via the amount of charge divided between amplifiers attached to the corners of the resistive anode. There are other continuous encoding mechanisms for MCPs including: 1) the Wedge and Strip anode 2) the Spiral Anode (SPAN), and 3) the Delay Line. Discrete anode structures, which use significantly more amplifiers and encode the location through direct detection, include: 1) the Multi-Anode Microchannel Array (MAMA), and 2) the capacitive readout system of the Coded Anode Converter (CODACON). There are still other methods for determining the location of the charge cloud emerging from an MCP. To facilitate a discussion of physical processes for state-of-the-art detectors, the present paper will focus on only two successful MCP detectors at the forefront of performance: the Delay Line

and the MAMA. Both of these detectors have recently undergone significant improvements.

There are several versions of Delay Lines being developed by various research groups. The basic principle of the Delay Line is straightforward. The charge cloud strikes an anode structure and two pulses begin propagating in opposite directions. The event position is encoded from the differences in the arrival times between these two charge pulses. Gas proportional counters have used Delay-Line readout systems for more than 25 years. This encoding technique was first used with MCPs by the Rutherford group, which used an anode of parallel wires coupled to a wire-wound delay line.

The Space Astrophysics Group at Berkeley has perhaps the most prodigious effort in Delay Line technology, making use of planar delay lines on a flat substrate. These Delay Lines are being developed for the Far Ultraviolet Spectroscopic Explorer (FUSE), the Orbital and Retrievable Far- and Extreme- Ultraviolet Spectrograph (ORFEUS), the Solar and Heliospheric Observatory (SOHO), and various sounding rockets. Early Delay Lines of planar design provided less resolution along the Y- than in the X- axis. New methods, however, may enable Y-axis event positions to be determined with about as much accuracy as the X-axis positions¹⁸. Currently, X-axis resolution of 20 μm is possible but with variations in resolution across the detector¹⁴. These Delay Lines overdigitize the event positions by about a factor of 10, providing the maximum retention of data resolution.

Unlike other continuous encoders, large format Delay Lines are readily possible since the position errors are small and only grow as the 1/3 power of the format size for a given gain³. This capability makes the Delay Line well suited for very long formats such as those required by the Rowland circle spectrograph on FUSE. It should be noted that curved focal planes are frequently desirable, especially for large formats and the Berkeley group has extensive experience using MCPs that have been polished to create a curved front surface. An advantage enjoyed by the Delay Line is the tube fabrication tolerances which are not nearly as tight as those for the competing MAMA detector system. These tolerances make the Delay Line relatively less difficult to fabricate. The principal shortcoming of the Delay Line as with any detector using a Z stack is the strong scene-dependent LDR. Gain sag is responsible for this LDR behavior and is well documented to be most pronounced for Z stack devices^{15,16}. Figure 4 shows the physical process responsible for this limitation. The Delay Line requires at least $2 \times 10^7 e^-$ to achieve $< 25 \mu\text{m}$ resolution¹⁹. To achieve this level of gain, a Z stack such as that shown schematically in Figure 4 must have charge spreading between each MCP so that numerous MCP channels are activated in the final plate for each event. If a second photoevent occurs in a time interval comparable to- or shorter than- the recharge time scale and within a distance comparable to the final charge cloud, the second event will have significantly less gain because some of the channels in the third plate that would have participated in the event are still depleted of charge. Thus, the centroid of the second pulse will have a systematic error. In the example of Figure 4, the second photoevent will either not be detected or will be erroneously displaced to the right, if it is detected.

This scene-dependent LDR behavior is not a major issue for many FUV and especially EUV applications where the flux levels are generally significantly lower than typical obser-

vations in the 1200 to 2000 Å wavelength interval. Further, certain optical designs sometimes mitigate the LDR problem for the Delay Line. The Rowland Circle Spectrograph on FUSE, for example, should constrain the light perpendicular to the dispersion direction, preventing to some extent charge depletion contributions from locations perpendicular to the dispersion. For other formats such as those of the STIS instrument, for example, this scene-dependent LDR would have been an important disadvantage. The tremendous gain required by a Z-stack detector also limits its lifetime as demonstrated by the Delay Line Detectors used on SOHO.

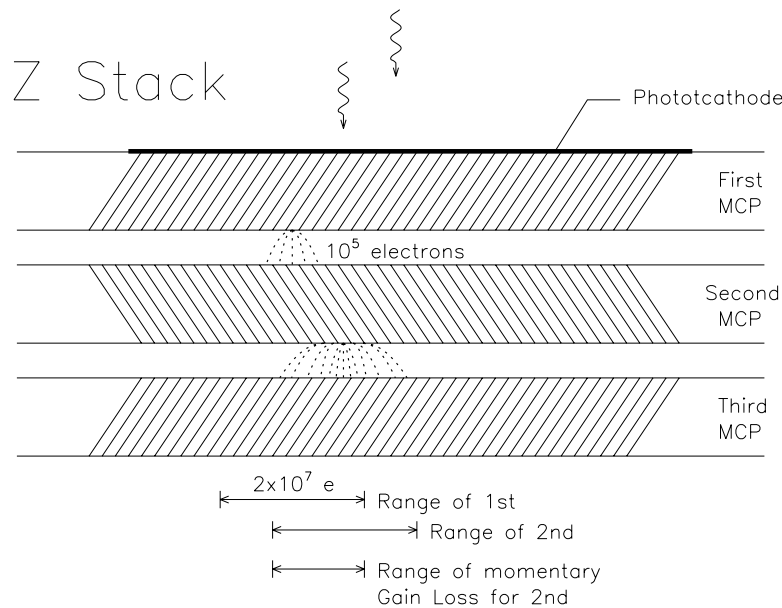


Fig. 4 showing the physical process responsible for the strong scene-dependent LDR for a Z Stack. All MCP detectors experience some loss of photometry and image distortion near their LDR limit, but these nonlinearities are significantly less for chevron stacks and even smaller for a single MCP^{15,16}.

For this and other performance reasons, the STIS project selected the Multi-Anode Microchannel Array (MAMA) detector. The STIS Instrument Team undertook a series of MAMA tube builds with improvements having been implemented at each stage to provide a sufficient heritage to insure fabrication success of the flight detectors. To date, some 16 working tubes have been produced, including 6 superb tubes meeting or surpassing flight specifications. The STIS detectors include several early prototypes that have been work horses for a number of years in the grating analysis facility at Goddard Space Flight Center. (It should be noted that a design flaw in the high voltage power supplies resulted in 2 flight tubes being destroyed. The design of the HV power supplies has been corrected.)

Two of the MAMAs have been launched on the second servicing mission to refurbish the Hubble Space Telescope.

As stated, the flight detectors exceed flight specifications in several important parameters. For example, the flight (BAND 1) CsI tubes have a maximum DQE of 21% compared to the 15% requirement while having a better visible light rejection than required. A logarithmic plot of the DQE sensitivity as a function from UV to visible wavelengths is shown in Figure 5.

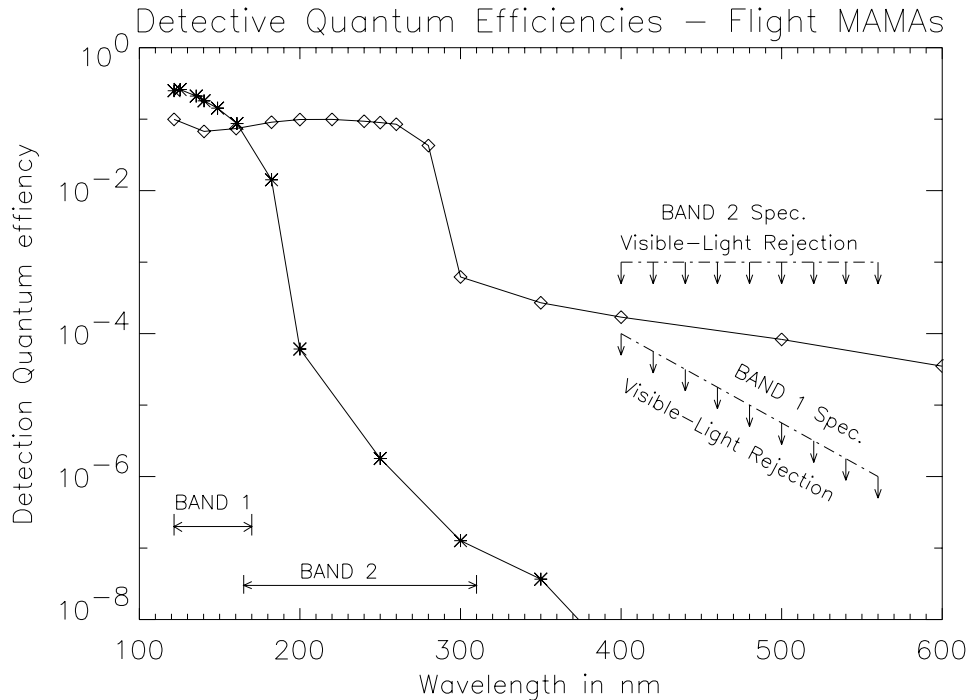


Fig. 5 showing the UV sensitivity and the visible light rejection as a function of wavelength for two MAMA Flight Tubes. Band 1 is the UV channel highlighted with "*" while Band 2 is the near-UV channel highlighted with open diamonds.

Environmental and life testing reveal these MAMA detectors to be robust and stable over long periods of time. Figure 6 shows the charge-extraction life testing of a typical Ni-Tec C plate used in the STIS MAMAs. The curves show the gain for various high-voltage settings as a function of the amount of charge extracted. The exponential reduction is the result of contaminants as well as the chemicals responsible for the electrical properties of the MCP being scrubbed out of the MCP and deposited, for example, on the anode structure. Fortunately the gain requirements of the MAMA are about 2 orders of magnitude below that needed by most MCP-based detector systems. The minimum gain requirements for efficient MAMA detector operation is shown as a horizontal dashed line corresponding to $2.0 \times 10^5 e^-$. The MCPs in the STIS MAMAs are preconditioned by extracting 1.0 Coulomb per square centimeter and another 0.5 to 1.0 $C cm^{-2}$ is expected to be extracted over the 5

year life of STIS. These data suggest the gain of the MAMA should be sufficient for much longer periods than the life of the Hubble Space Telescope and provide very stable performance.

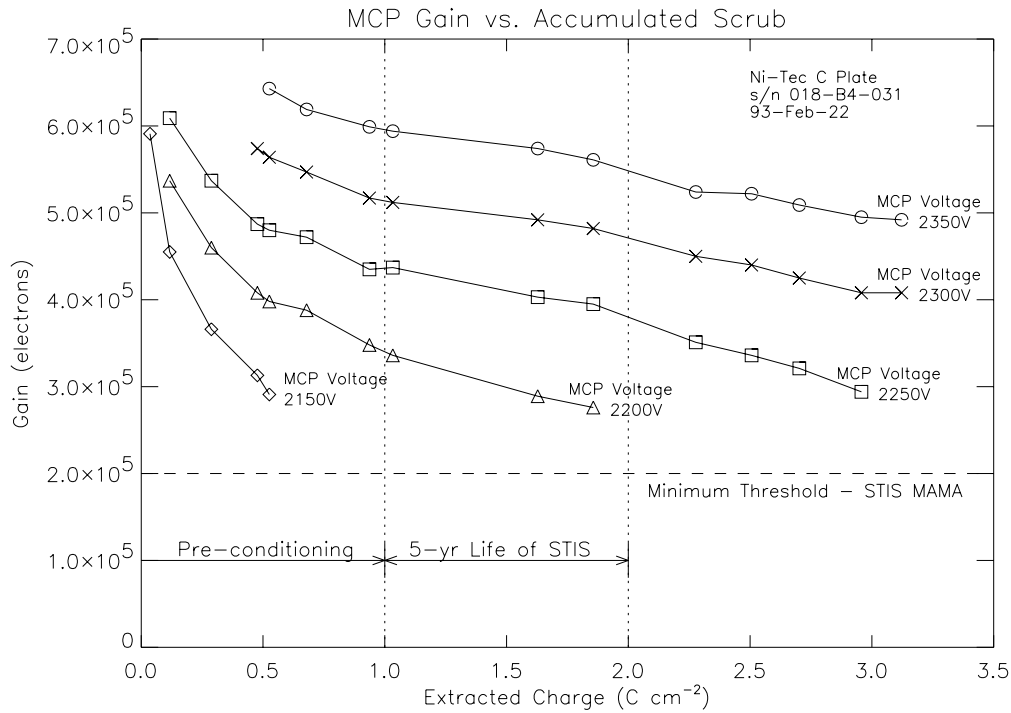


Fig. 6 showing the gain life of the MCP as a function of extracted charge which is a measure of the total MCP usage. The small gain requirements for MAMA detectors allows the MCP to be preconditioned to a much greater degree and operate more stably over greater periods of time than a detector using a Z stack.

Other testing demonstrated the MAMA to be robust against over-light conditions. Figure 7 is a cross-sectional plot through an image with a diameter of about 15 pixels (375 μm). Images 15-pixels wide provide a more severe test for MCPs than those 1-2 pixels wide since gain sag occurs not only in the MCP pore of interest but in adjacent pores as well, which otherwise might help to replenish the charge. As can be seen in Figure 7, the Output/Input count rate efficiency remains very linear for rates upto about 200 counts/pixel/second, a factor of 4 above specification. At higher rates, the gain sag becomes significant and the output rate falls despite the higher input rate. Nevertheless, this behavior is localized to the immediate region of the bright spot, leaving all remaining area of the detector unaffected. No increase in the dark rate nor any type of persistence is observed immediately after the image is removed. In addition, the STIS team placed a localized spot on an engineering detector at a count rate of 50 c/p/s and extracted 1 Coulomb cm^{-2} in that region. Comparison flat fields taken before and after this spot test reveal no depression in sensitivity at the spot location. For excessive flux levels (> 1000 c/p/s) maintained over substantial periods (> 2000 s), permanent gain losses do start to occur and become important at count

rates of 10,000 c/p/s over extended periods of time. These detectors are thus remarkably stable since the detectors require an over light condition of more than a factor of 20 above specification and for substantial periods of time to show any measurable effect.

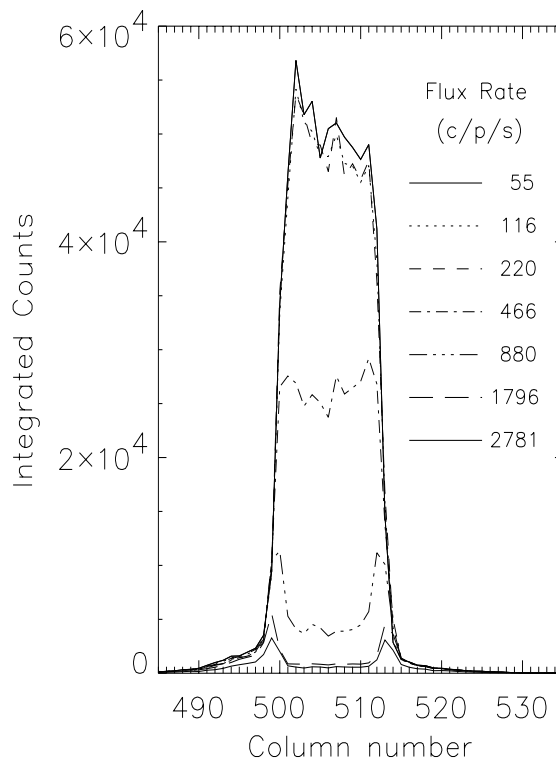


Fig. 7 showing the detector response to an image that is many times brighter than the local dynamic range. Localized charge depletion within the MCP at the location of the image causes a temporary loss in counting efficiency leaving the rest of the detector unaffected. This test also demonstrates the safety and robustness of the MAMA detector to extremely bright stars observed in imaging mode. No persistence nor gain loss is observed immediately after the image is removed.

3. ELECTRON-BOMBARDED CCDs (EBCCDs)

Electron-Bombarded CCDs (EBCCDs) have been under development for a number of years at Princeton University, the Naval Research Laboratory, and other research centers^{11,21}. One EBCCD with an opaque photocathode has been used in the Interstellar Medium Absorption Profile Spectrometer (IMAPS) sounding rocket, which also successfully flew piggyback twice on ORFEUS Mission.

The IMAPS detector, which is shown schematically in Figure 8, is described extensively in Jenkins¹¹ for the old magnet assembly. The magnet assembly shown in Figure 8 is a novel design produced by the US Army Electronics Technology and Devices Laboratory and is under development at Princeton Scientific Instruments. The EBCCD basically consists of a photocathode surface, an accelerating electrostatic field of several thousand volts to accelerate the photoelectrons, and a thinned, backside illuminated CCD. A photoelectron striking the CCD produces approximately one secondary electron for every 3.6 eV of incident energy. In practice, photoelectrons in the IMAPS detector having 18.5 KeV pass through a 3 KeV dead layer, producing approximately 3,000 electron-hole pairs. Each photoevent is localized

in a width having an exponential (rather than Gaussian) spread with a scale length of 4-6 μm in the CCD. The entire CCD image is read at a rate of 15 hertz and individual photo-events identified. The CCD is operated warm with a dark level of 1500-7500 electrons and a readout noise of 70 electrons. The EBCCD with an opaque photocathode on a smooth surface achieves the highest quantum efficiency currently available ($\text{DQE} > 70\%$)¹¹. A magnetic field is required to shift the photoelectrons out of the optical path and towards the CCD as shown in Figure 8.

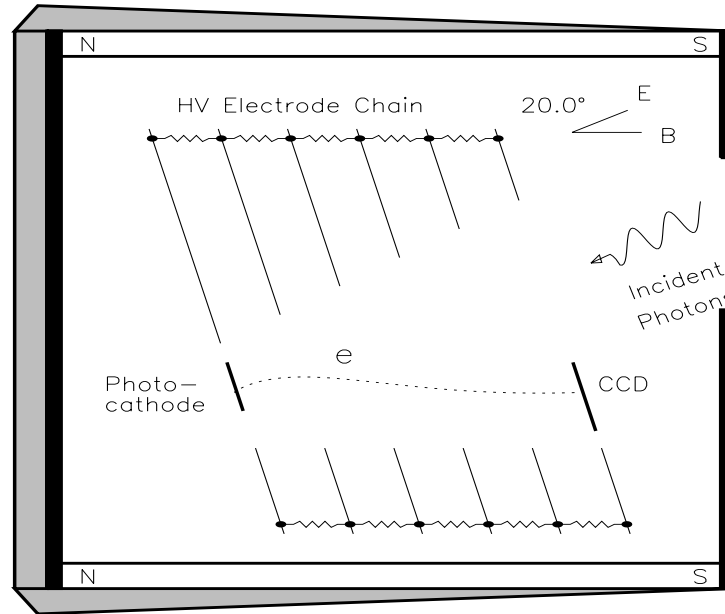


Fig. 8 schematic diagram of the Electron-Bombarded CCD (EBCCD), which has flown successfully on sounding rockets and on the ORFEUS orbital mission. The EBCCD offers the highest QE from a photocathode. New cladding magnets shown as gray shaded regions allow a reduction in weight by a factor of 3

The new magnet assembly shown in Figure 8 will result in a factor of 3 reduction in weight. Field uniformity and flux confinement are attained with minimal structural mass through the principal of permanent magnet cladding²¹ The primary magnetic field is established through supply magnets shown as two horizontal white bars labeled with "N" and "S" in Figure 8. The black pieces are iron bars used as flux conduits. The cladding magnets are shown as gray shaded regions. The poles of these cladding magnets are all toward the center and the strength is proportional to the thickness of the "wedge". This creates the equivalent of an equipotential outer surface, forcing all the flux from the source magnets into the detector cavity. The magnet assembly has minimal flux outside of the detector and a more uniform field inside it. Cladding magnet assemblies are so efficient that one

cannot use the structure of an optimal design since it does not provide sufficient mechanical strength.

As already noted, the primary advantage of the EBCCD is its high DQE ($>60\%$), a factor of 2-3 above the values that can be obtained with MCP detectors. The Local- and Global- Dynamic Range envelopes, shown in Figure 3, are also important strengths. The IMAPS EBCCD is simultaneously capable of photon-counting detection and analogue mode operation for high flux levels where event crowding occurs for the 1/15 second frame rates. In the latter mode, the signal from multiple photoevents is converted analog-to-digitally and the signal added to the existing signal in an integrating memory. If ions enter the detector, or are created therein, these will be accelerated toward the photocathode, creating 10 to 20 free electrons. These electrons will be electromagnetically focused onto the CCD within about a pixel size and are easily discriminated out.

4. GaAlN AND GaN DETECTORS OF THE FUTURE

Another technology under development that holds real promise for UV image sensors are photoconductive detectors based on GaN or GaAlN substrates^{12,13}. The band gap between valence and conduction bands is much larger for these substrates than for silicon, making these devices inherently superior for UV applications. Compared to conventional silicon-based CCDs, GaAlN detectors are expected to present the following advantages: solar blindness, high quantum efficiency in the UV, and low dark current/low noise. Compared to image sensors using a photocathode, solid-state detectors present the advantages that have already been clearly demonstrated by Silicon CCDs: high spatial resolution, robustness, light weight, and large dynamic range. GaAlN or GaN solid state detectors also do not require high voltages which are always an inherent failure risk.

Compared to SiC, another wide bandgap semiconductor candidate, GaAlN presents the following advantages: 1) a direct bandgap resulting in a high absorption coefficient, 2) a sharper cut-off, 3) a higher response speed, and 4) the possibility of making heterojunction devices which will result in improved quantum efficiency. In addition, there is the ability to tailor the cut-off wavelength by varying the GaAlN alloy composition. The detectors made with these materials appear to be $> 80\%$ efficient at near-UV wavelengths^{12,13}, be tailored to a specific long-wavelength cutoff between $\sim 3600\text{\AA}$ and $\sim 1900\text{\AA}$, and can be operated at temperatures near 20°C .

These detectors are, however, in their infancy. While much of the initial data are very promising, there remain a number of parameters that still need to be explored. For example, DQE curves have been measured showing peak performance of about 90% near 250 nm with a visible light response of 2 to 4 orders of magnitude less^{12,13}. However, one really needs to obtain or verify a visible response that is 5 to 8 orders of magnitude less than the peak sensitivity, similar to the curves in Figure 5. This requirement is driven by the fact that many astronomical objects emit 10^4 to 10^8 photons at visible wavelengths for every UV photon. A rejection of only 4 orders of magnitude at visible wavelengths would still require heavy filtering and corresponding loss of UV DQE. It is likely the GaN or GaAlN have

much better rejection properties, but simply have not been measured adequately. Similarly, the ultimate response to low-light-level illumination is not known nor is the response to wavelengths below about 180 nm. All of these parameters will be measured soon and one can expect significant progress in device fabrications over the next few years.

5. REFERENCES

1. Carruthers, G.R. 1993, Chapter 15 entitled: "Ultraviolet And X-Ray Detectors", in *Electro-Optics Handbook*, R.W. Waynant & M.N. Ediger, editors, McGraw-Hill Inc.
2. Joseph, C.L. 1995 *Experimental Astronomy*, 6, 97. invited review
3. Lampton, M.L. 1991, invited review for *Extreme Ultraviolet Astronomy*, R.F. Malina and S. Bowyer, eds., (New York: Pergamon Press).
4. Timothy, J. G. 1991a, invited review in *Photoelectronic Image Devices 1991*, ed. B.L. Morgan, Institute of Physics Conference Series No. 121, p.
5. Siegmund, O.H.W., Gummin, M.A., Stock, J., & Marsh, D. 1992, in *Proc. of an ESA Symp. on Photon Detectors for Space Instrumentation*,
6. Wilson, B., editor 1991, "Workshop Proceedings: Sensor systems for Space Astrophysics in the 21st Century", *Astrotech 21 Series III*, JPL Publication 91-24, Vol 3.
7. Welsh, B.Y. 1992, in *Proceedings of an ESA Symp. on Photon Detectors for Space Instrumentation*, held at ESA/ESTEC, Noordwijk, The Netherlands, 10-12 November 1992. (ESA SP-356, Dec. 1992).
8. Joseph, C.L. Argabright, V., Bybee, R., Danks, A., & Woodgate, B. 1994, *Proc. SPIE Ultraviolet Technology V*, 2282, 116.
9. Joseph, C.L. Argabright, V., Abraham, J., Dieball, D., Franka, S., Styonovich, M., Van Houten, C., Danks, A., & Woodgate, B. 1995, *Proc. SPIE Ultraviolet Technology V*, 2551, 248.
10. Siegmund, O.H.W., & Gaines, G.A. 1990, *SPIE, EUV, X-ray and Gamma-ray Instrumentation in Astronomy*, 1344, p. 217.
11. Jenkins, E.B., Joseph, C.L., Long, D., Zucchino, P.M., Carruthers, G.R., Bottema, M., & Delamere, W.A. 1988, *SPIE Ultraviolet Technology II*, 932, p. 213.
12. Razeghi, M. *et al.*, 1995 *Appl. Phys. Lett.* 67, 1745.
13. Kung, P., Zhang, X., Walker, D., Saxler, A., Piotrowski, J., and Razeghi, M. 1995, *Appl. Phys. Lett.* 67, 18.

14. Siegmund, O.H.W., Gummin, M.A., Stock, J., Marsh, D., Sasseen, T., Raffanti, R., & Hull, J. 1994a, Preprint entitled: "Delay line microchannel plate detectors for the Far Ultraviolet Spectroscopic Explorer Satellite."
15. Fraser, G.W., Barstow, M.A., and Pearson, J.F. 1988, *Nucl. Instr. Meth.*, A273, 667.
16. Fraser, G.W., Pain, M.T., & Lees, J.E. 1993, *Nucl. Instr. Meth. in Physics Research*, A327, 328.
17. Dopita, M.A. 1994, "The Starlab/Endeavor Photon Counting Array Detector: Capabilities for use in the UV detector of Advanced Camera". A report to the JPL Advanced Camera Science Advisory Committee.
18. Raffanti, R. & Lampton, M. 1993, *Rev.Sci.Instrum.*, 64(6), 1506.
19. Siegmund, O.H.W., Lampton, M.L., & Raffanti, R. 1989, *Proc. SPIE*, 1159, 476.
20. Joseph, C.L., Argabright, V., and Bybee, R. 1997, in preparation.
21. Lowrance, J.L., Joseph, C.L., Leupold, H., & Potenziani, E. 1991, in *Photoelectronic Image Devices 1991*, ed. B.L. Morgan, Institute of Physics Conference Series No. 121.